ChemComm

FEATURE ARTICLE

View Article Online
View Journal | View Issue

Cite this: *Chem. Commun.*, 2025, **61**, 8157

Operando characterization technique innovations in single-atom catalyst-derived electrochemical CO_2 conversion

Syed Asim Ali,[ab] Iqra Sadiq[a] and Tokeer Ahmad *[a]

Received 10th March 2025,
Accepted 6th May 2025

DOI: 10.1039/d5cc01287b

rsc.li/chemcomm

Single-atom catalysts (SACs) are the perfect epitome of cutting-edge innovation in catalysis, offering distinct active sites in the form of isolated, individual atoms. SACs amalgamate the advantages of homogeneous and heterogeneous catalysis, in turn enhancing the activity, selectivity, and stability during catalytic processes. The latest progressions in *in situ*/*operando* characterization techniques have simplified the understanding of the catalyst heterogeneity and structure sensitivity of SACs by enabling the real-time observation of SACs under a coexistent working environment to provide insights into their structure and catalytic efficiency. *Operando* techniques are the backbone for investigating the stability and activity of SACs during energy conversions. Techniques such as *operando* X-ray absorption spectroscopy (XAS), polarization-modulation infrared reflection absorption spectroscopy (PM-IRAS), and near-ambient-pressure X-ray photoelectron spectroscopy (NAP-XPS) have been employed to study SACs under different reaction conditions. Furthermore, *in situ* visualization microscopy techniques have made notable progress in the imaging of ongoing catalytic reactions on SACs and revealed enigmatic effects such as facet-resolved catalytic ignition and anisotropic surface oxidation. Therefore, in this review, we have compiled the developments in the significant *operando* characterization techniques for SAC-derived electrochemical carbon dioxide reduction reaction (eCO_2RR).

Introduction

The last decade has witnessed an unprecedented pace in heterogeneous catalysis with the advent of a pioneering class of materials, notably transition metal carbonitrides (MXenes) and SACs. The research findings of MXenes are relatively more pronounced and significant knowledge of these two-dimensional (2D) materials has been harvested as compared to SACs.[1,2] However, the fabrication

[a] *Nanochemistry Laboratory, Department of Chemistry, Jamia Millia Islamia, New Delhi, 110025, India. E-mail: tahmad3@jmi.ac.in; Tel: +91-11-26981717 ext. 3261*
[b] *Department of Inorganic and Organic Chemistry, Inorganic Chemistry Section, University of Barcelona, Carrer de Martí iFranquès, 1-11, 08028 Barcelona, Spain*

Syed Asim Ali

Dr Syed Asim Ali is a postdoctoral researcher at the University of Barcelona, Spain in the Department of Inorganic Chemistry and is currently working on exploring magnetic properties of metallic nanowire-based photocatalysts. His research interests include designing advanced functional materials and their operando/ex situ characterization, energy conversion applications specifically hydrogen evolution, CO_2 reduction and nitrogen fixation reactions, computational chemistry and techno-economic analysis.

Iqra Sadiq

Iqra Sadiq, after graduating from K. R. Mangalam University, completed her post-graduation from G. D. Goenka University, Gurugram, joined Jamia Millia Islamia University, New Delhi as a research scholar under the supervision of Prof. Tokeer Ahmad and is currently working on the chemical synthesis and structural characterization of some functional nanostructures for environmental remediation and energy-based applications.

of state-of-the-art MXene/MBene-based materials and their upscaling require a comprehensive mechanistic knowledge of the optimized synthetic protocols, etching/exfoliating parameters, and participatory intercalation/delamination steps.[3] Conversely, the progress of SACs is incongruent with that of MXenes and is still in its embryonic stage. SACs have garnered considerable attention from researchers supported by the advancements in methodological developments, characterization tools, and machine learning. In contrast to homogeneous catalysis, wherein nearly one hundred percent metal atom harnessing can be achieved subject to the reaction conditions, heterogeneous catalysis has its limitations due to the aggregation of catalytically active sites, which in turn obscures the active centres. Catalytically active surface sites, such as apices and edge/corner/step-sites, of the catalyst surface only account for nearly 20 mol% of the available mass.[4,5] Therefore, designing SACs externalizes the enduring objective of researchers to reach higher atom utilization efficiency. Reaching nearly unity atomic efficiency can bring about the predominance of homogeneous as well as heterogeneous catalysis. Nevertheless, the facile synthesis of SACs is hampered by the non-achievement of the enhanced single-atom loading on account of the Gibbs-Thomson limit, which highlights the challenges of reaching higher than 3 mol% loading.[6]

The term SAC was first coined by Zhang and coworkers,[7] manifesting the reasonably higher atom efficiency of single Pt atoms dispersed over FeO_x, resulting in facilitated CO oxidation. The emergence of SAC-derived heterogeneous catalysis is eventuated due to the latest innovations in *operando* characterization techniques and robust computational modelling.[8,9] The amalgamation of these two indispensable tools allows precise insights into the atoms' dispersion, structural evolution, and precise location during *in situ* dynamics. There are several well-known chemical transformations in which dispersed metal atoms are present over a supporting material, such as olefin chemisorption or metallic complexes over porous materials such as zeolite.[10]

Tokeer Ahmad

Prof. Tokeer Ahmad (graduated from IIT Delhi) is full Professor of Chemistry at JMI Delhi. Prof. Ahmad has supervised 16 PhDs, 84 postgraduates, 10 projects, published over 225 research papers, one patent and three books with research citation of over 9570. Prof. Ahmad is the recipient of CRSI Bronze Medal, MRSI Medal, SMC Bronze Medal, ISCAS Medal, Inspired Teacher's President of India Award, DST-DFG award, Distinguished Scientist Award, Maulana Abul Kalam Azad Excellence Award of Education, Teacher's Excellence Award, elected as Member of National Academy of Sciences India, and has also been admitted as Fellow of the Royal Society of Chemistry (FRSC), UK.

Therefore, several studies in the past hinted at the superiority of isolated atomic sites in catalysis over a molecular catalyst ensemble of different molecules.[11] However, SACs specifically differ from these earlier reactions and have no interactions with small organic groups or ligands.[12] The synthesis of SACs *via* the metal coordination route has been realized very recently, thus paving the way for unconventional methodologies for the scalable synthesis of SACs.[6] For instance, Duan *et al.*[6] reported an ultrahigh metal loading as high as ~16 mol% over a C_3N_4 support in a facile synthesis through one-pot metal coordination. The group exploited the accelerated complexation of ligand molecules/metal ions and their eventual *in situ* polymerization to form ultrahigh Cu-loaded SACs for CO_2 photoconversion into formic acid. The scalable applicability of SACs is repeatedly questioned, ascribed to their susceptibility to aggregation before the activation and reaction steps. An ever-growing amount of research on SACs suggests the superior stability of metal atoms bonded to the support material through covalent bonding, in contrast to the nanoparticle analogue.[13,14] The thorough examination of SACs in discrete environmental conditions *via in situ* techniques is significant for understanding their dynamics, and it led to the origination of the field of "dynamic single-atom catalysis" that focuses on the dynamic conversion of nanoparticles into SACs during catalytic transformations.[15,16] Computational modelling has played an important role in understanding the dynamics in SACs. The agglomeration of Pt SACs into nanoclusters has been observed upon CO exposure, and their subsequent conversion into SACs has been documented after the removal of CO molecules.[17] The stable (111) facets of Cu-SAC have been proved to undergo dynamism by etching and subsequent breaking into nanoparticles attributed to their interaction with CO molecules.[18] These reports corroborate the effect of CO adsorption in the dynamics of the agglomeration of SACs into nanoparticles and necessitate the utilization of *in situ* and *ex situ* characterizations of SACs to determine their role during heterogeneous catalysis, specifically in CO_2RR.

Low-metal-loaded catalysts dispersed on a supporting material have fascinated researchers for the past few decades. However, the lack of *in situ*/*operando* characterization tools limited the comprehensive understanding at that time and one could not probe the distinction between single-atom and cluster sites. Through the innovations in spectroscopic tools, it has now been well substantiated that decorating metal atoms on a supporting material efficiently tunes their catalytic performance in a certain way.[19,20] *In situ operando* techniques have been instrumental in advancing the understanding of catalytic processes involving SACs, offering valuable insights into their physicochemical characteristics and dynamic phase transitions. The development of a methodological framework for investigating the structural and electronic properties of SACs has ensured their efficient real-time monitoring.

Early reports have underscored the utilization of XAS to investigate the ability of SACs in heterogeneous catalysis.[21] Researchers have exploited the extended X-ray absorption fine structure (EXAFS) technique to probe dispersed Pt atoms for enhanced propane combustion. This benchmark set the tone

for successive studies by employing acid washing to preserve SACs in the catalytic system.[22,23] However, the mechanistic scheme during catalytic reactions is vague, and researchers are stepping forward to examine the atomic lattice at better resolution *via* different characterization techniques. For instance, environmental transmission electron microscopy (ETEM), which aids in visualizing reaction steps, has been upgraded to environmental scanning TEM (ESTEM) to provide sub-angstrom resolution with precise analysis of SACs. ESTEM is an important *operando* tool for the real-time analysis of single atoms deposited over light support materials at higher temperature ranges.[24,25] *Operando* analysis provides significant insights into the different intermediate species formed during the SAC-derived CO_2RR mechanism.

In situ visualization of SACs

In recent years, several *operando* techniques have been developed to elucidate the dynamics in SACs, probe their stability against aggregation, and determine the reaction mechanism of SAC-derived energy conversion processes.[26,27] *In situ* visualization of SACs plays a fundamental role in comprehending their structure, stability, and catalytic mechanisms under actual working conditions. Given the atomic-scale dispersion of active sites in SACs, advanced imaging and spectroscopy techniques are crucial to visualize and characterize them at the atomic level. For instance, aberration-corrected TEM, ETEM, and scanning transmission electron microscopy (STEM) have played a vital role in the visualization of SAC dynamics. For determining the active sites of SACs in heterogeneous catalysis, *operando* imaging is an important tool that elucidates the mechanism of particular transformations. In recent years, electron microscopic techniques have improved tremendously, thus enabling researchers to demonstrate the rapid reactions attributed to the accessibility of direct electron detectors and improvement in the image-taking technologies to capture more frames per second.[26] Researchers have exploited *in situ* imaging techniques to analyse the dispersion of SACs over support materials. For instance, Wei *et al.*[28] probed the thermal transformation of noble metal nanoparticles (NPs) to their corresponding SACs on a metal–organic framework (MOF)-based support material. The group successfully observed the accumulation of noble metal NPs during thermal heating (1000 °C) on account of the rearrangement of the NPs to lower the overall free energy. *In situ* visualization showcased the thermal mobility and high-impact collisions of the bigger NPs with the support material, facilitating Pd NPs' atomization. Based on these results, the authors corroborated the essential requirement of high-angle annular dark-field (HAADF)-STEM visualization to capture the collision between metal NPs and the interior of the support material and the different intermediary steps as TEM analysis was not able to prove the emergence of Pd single atoms owing to its phase contrast shortcomings. HAADF-STEM is instrumental in obtaining Z-contrast images in which the intensity of every atomic column is in proportion to its atomic number. Therefore, with this technique, direct imaging of monodispersed or aggregated single atoms on a support material is possible, allowing one to distinguish SACs from NPs. Therefore, this report highlighted the significance of HAADF-STEM in proving the formation of SACs and the conversion of NPs to SACs based on the heating profile. Recently, Wang *et al.*[29] developed a unique negative pressure annealing (NPA) methodology to prepare exceptionally high-metal-loaded SAC@gC_3N_4 systems for a wide range of metals. Conventional fabrication routes usually struggle to attain metal loading above 10 wt% due to challenges like metal aggregation and high entropy of single atoms. In contrast, this study introduces an NPA strategy that successfully fabricates SACs with metal loadings ranging from 27.3 to 44.8 wt% over a gC_3N_4 array. For probing ultrahigh metal loading, the group exploited the *operando* aberration-corrected HAADF-STEM (AC-STEM) technique to determine the significant role of NPA in the removal rate of anionic species present in the metal sources and in boosting the interaction of single atoms with N-defect sites. The latter process underscores the strong bonding between the single atoms and the N-rich gC_3N_4 matrix. The group ascertained that increasing the Pt loading (41.8 wt%) over gC_3N_4 led to enhanced catalytic efficiency toward propane oxidation to yield higher carbon products. AC-STEM analysis was carried out to demonstrate the local environment of Pt single atoms as illustrated in Fig. 1(a) and (b). The decoration of monodispersed Pt atoms is represented by the bright spots in the dark background of gC_3N_4. Furthermore, the authors also examined the temperature-dependent AC-STEM images of ultrahigh Pt-loaded gC_3N_4 in vacuum and Ar conditions to elucidate the structural evolution of Pt precursor during the annealing operation as depicted in Fig. 1(c) and (d). Densely dispersed bright spots were evident at low temperatures, signifying the homogeneously distributed Pt source. Furthermore, cluster/particle formation was not observed even on increasing the temperature and the Pt SACs were not observed as revealed in Fig. 1(c). However, negative annealing under Ar flow resulted in the formation of Pt single atoms on increasing the temperature and the Pt atoms were well scattered at 400 °C as shown in Fig. 1(d). Therefore, the combined results of *in situ* analysis revealed the high metal loading of SACs over gC_3N_4. However, the NPA methodology should be tested for different support matrices such as TiO_2 or MOF materials to shed light on the bonding between single atoms and defective-coordinated sites of a support material. It has been observed that annealing at ambient pressure gives rise to unwanted cluster formation of single atoms. Therefore, to tune the aggregation of single atoms *via* pressure lowering, Al-Hilfi *et al.*[30] introduced a viable methodology to design high-density SACs for scalable production by manipulating metal diffusion during a pyrolysis process through pressure control. The group demonstrated the role of pressure reduction in enhancing metal diffusion, thus reducing the aggregation of atoms during pyrolysis.

In theory, operating at high-vacuum or low-pressure conditions reduces the collision rate during the interaction of single atoms with the support material. This idea nurtured the exploitation of pressure-controlling by the group to enhance the loading of SACs on N-graphitic carbon substrate. Fig. 1(e) and (f) clearly distinguishes between the morphology of Fe single atoms at ambient and low-pressure conditions. The group exploited HAADF-STEM images to determine the role of pressure reduction in ultrahigh Fe loading and varied the

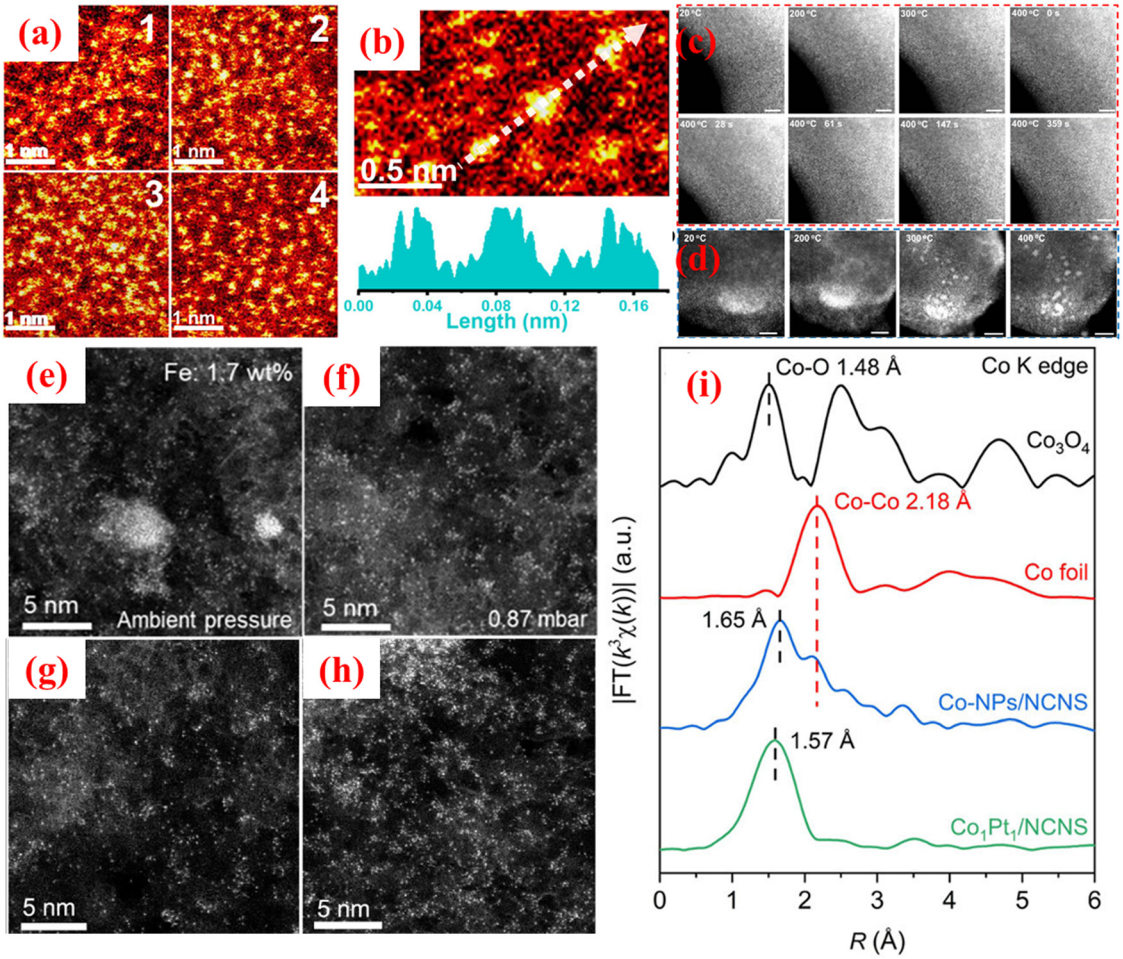

Fig. 1 AC-STEM images of Pt@gC_3N_4 at (a) 1 nm scale and (b) 0.5 nm scale. Temperature-dependent *operando* AC-STEM images of (c) Pt SACs@gC_3N_4 and (d) Pt NPs@gC_3N_4. Reproduced with permission from ref. 29. Copyright 2024, Springer Nature. Morphological variations of Fe single atoms on N-graphitic carbon substrate (Fe-NC) at (e) ambient pressure and (f) 0.87 mbar. AC-HAADF-STEM images of (g) $Fe_{0.1}$-$NC^{0.87}$ and (h) $Fe_{0.2}$-$NC^{0.87}$. Reproduced with permission from ref. 30. Copyright 2024, American Chemical Society. (i) EXAFS of CoPt single atoms, Co-NPs, Co-foil, and Co_3O_4 at Co K edge. Reproduced with permission from ref. 31. Copyright 2021, Springer Nature.

pressure from 1.4 to 0.14 mbar. As shown in Fig. 1(g) and (h), significant Fe atom decoration can be seen at the optimized 0.87 mbar pressure conditions. The same experiments were repeated for different noble and non-precious metals to determine the effect of pressure-controlled metal diffusion. This study steps forward toward the scalable production and broader application of dense SACs in heterogeneous catalysis.

X-ray absorption spectroscopy (XAS)

The XAS technique has emerged as an element-definite approach to specifying the elemental properties of a wide range of advanced materials.[19] As SACs consist of transition metals, *in situ* XAS can detect the elemental-specific properties at very low concentrations under actual electrochemical or photochemical CO_2RR conditions. XAS's sensitivity to elements facilitates its application in determining the oxidation states and localized electronic properties of single metal atoms to elucidate the active centres during CO_2 reduction. For adequately monitoring SACs during CO_2RR, the XAS technique is a crucial method that can identify variations in oxidation states/coordination environments during the reaction process and provides better insights into product selectivity through the correlation of spectral features. XAS allows the precise analysis of active sites in SACs without interference from the support material, offering detailed information on the local atomic environment, including bond lengths and coordination numbers.[5] XAS works excellently with non-crystalline/highly dispersed SACs where conventional crystallographic techniques such as X-ray diffraction fail. It permits the real-time monitoring of SAC behaviour during specific catalytic transformations and can be performed under certain reaction conditions concerning temperature, pressure, and gas environment. XAS complements other *in situ* characterization methods to comprehensively understand SAC properties. However, several challenges limit the large-scale applicability of XAS for SAC investigations. For instance, high-quality XAS measurements typically require expensive synchrotron radiation sources, and they provide an ensemble average of the atomic environment, which can obscure subtle differences in heterogeneous SAC systems.[32] Prolonged exposure to hard X-rays can cause radiation-induced changes in SACs. EXAFS and

X-ray absorption near edge structure (XANES) are subsets of XAS. These techniques are extremely important to confirm the monodisperse nature of SACs. As compared to EXAFS, XANES provides more consolidating evidence regarding the environment, distortion and electronic structure of single atoms due to its relatively superior signal-to-noise ratio, thus resulting in its suitability for *in situ* investigations.[33] On the other hand, EXAFS findings are frequently affected by the lower metal loading or signal attenuations from the surroundings. Despite the extensive utilization of the XANES technique for *operando* analysis, its complicated fitting processes and time-intensiveness hinder its use in quantitative SAC characterization. Nevertheless, recent advancements in computational modelling taking into consideration XANES data have improved its feasibility for *in situ* studies.[34,35] The basic distinction between XANES and EXAFS is that the former determines the electronic states of single atoms and emerges through the excitation of core electrons to the valence and conduction bands. In contrast, the latter is based on scattering effects between photo-induced electron carriers with the surrounding single atoms, and thus is useful for determining 3D geometry. The findings from XAS measurements have sharpened the understanding of SACs as corroborated by recent reports.[36] For instance, Li *et al.*[31] presented an innovative strategy for synthesizing Co/Fe/Ni-based single atoms with a pyrrolic-N_4 coordination structure. This unique methodology utilized Pt atoms to catalyze the formation of Co/Fe/Ni-SACs coordinated with four pyrrolic N atoms, forming a stable pyrrolic-N_4 structure as confirmed by XAS observations. The authors used the XANES simulations and EXAFS investigations to probe the M-coordinated pyrrolic-N_4 geometry. The formation of Co single atoms was confirmed by EXAFS analysis which revealed the peak ascribed to the first shell of the Co-coordinated site with the heteroatom at 1.57 Å, thus implying the existence of Co-SACs as shown in Fig. 1(i). Moreover, the absence of a Co–Co peak bolstered the evidence for the formation of Co-SACs over NPs. In addition, to demonstrate the local surrounding structure of as-prepared SACs, the authors utilized XANES analysis that underscored the agreement with the XPS results, indicating the +2 oxidation state for Co single atoms. A schematic representation of the XAS characterisation setup in transmission, fluorescence, and total electron modes can be seen in Fig. 2(a)–(c). Fig. 3(a) illustrates the significant change in the XANES spectra of Co-SACs compared to Co foil and Co_3O_4 reference. This study provides an effective strategy for preparing pyrrolic-N_4-type SACs for energy conversion applications, especially for HER/OER processes.

Near-ambient-pressure X-ray photoelectron spectroscopy (NAP-XPS)

NAP-XPS is an advanced variation of XPS that allows surface chemical analysis of SACs under near-realistic conditions, including gases, liquids, and elevated pressures. In contrast to traditional XPS that functions at ultrahigh-vacuum conditions, NAP-XPS can reach a pressure limit of up to a few tens of mbar, thus making it an important technique for *in situ*/*operando* studies and real-time reaction monitoring. NAP-XPS is capable of differentiating single-atom dispersions from NPs by investigating metal coordination and electronic states.[41] Muravev *et al.*[42] fabricated Pd single atoms decorated on CeO_2 for CO oxidation investigations *via* an impregnation/spray pyrolysis methodology. The authors utilized *in situ* NAP-XPS to underscore the enhanced stability of Pd-SACs through significant Pd–CeO_2 bonding. The NAP-XPS studies provided the surface electronic properties of Pd–CeO_2 *via* bonding elucidation through the 3d core-level spectrum of Pd. Two different Pd electronic states were observed at 50 °C during the CO oxidation process, showing the main peak of Pd–O_x–Ce type of bonding, whereas the low-intensity peak was ascribed to the minimal PdO_x aggregation. These results corroborate the higher stability of Pd–CeO_2 even at high temperature (300 °C) due to the peak retention. Impeng *et al.*[37] constructed Cu single atoms on a UiO-66 MOF support and explored its catalytic efficiency toward preferential oxidation

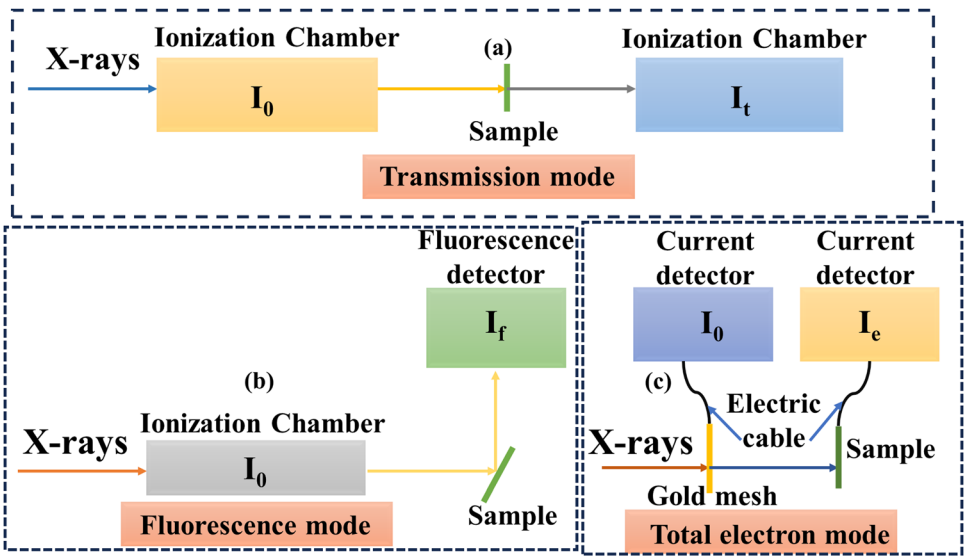

Fig. 2 Schematic representation of XAS characterisation setup in (a) transmission, (b) fluorescence and (c) total electron modes.

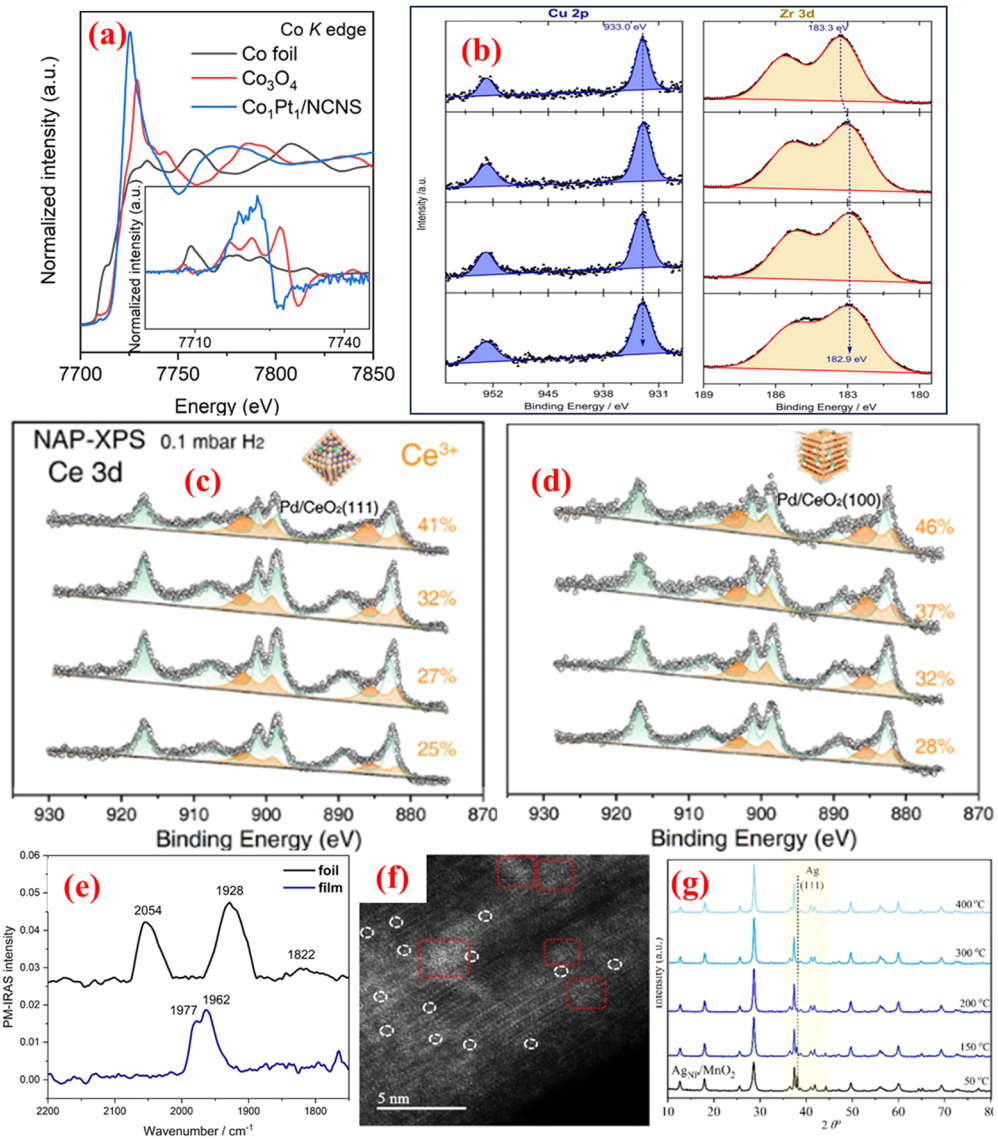

Fig. 3 (a) XANES spectra and first derivative curves (inset) of Co_1Pt_1 single atoms and reference samples. Reproduced with permission from ref. 31. Copyright 2021, Springer Nature. (b) NAP-XPS of Cu 2p and Zr 3d at 250 °C and 2 mbar in different reaction conditions. Reproduced with permission from ref. 37. Copyright 2024, Royal Society of Chemistry. NAP-XPS of Ce 3d in (c) Pd/CeO_2(111) and (d) Pd/CeO_2(100). Reproduced with permission from ref. 38. Copyright 2022, John Wiley and Sons. (e) PM-IRAS spectroscopy of CO adsorption over a Pd LCC catalyst. Reproduced with permission from ref. 39. Copyright 2024, Springer Nature. (f) HAADF-STEM image of AgNP/MnO_2-350. Isolated Ag atoms are circled in white, Ag clusters in red rectangles. (g) *In situ* XRD patterns of AgNP/MnO_2 at distinct temperatures. Reproduced with permission from ref. 40. Copyright 2021, John Wiley and Sons.

of CO in the presence of H_2. *In situ* characterization techniques such as XANES and NAP-XPS revealed that increasing the temperature led to a higher proportion of Cu^{1+} single atoms and partial reduction of ZrO_x nodes. NAP-XPS spectra of core line Cu 2p and Zr 3d at 250 °C are illustrated in Fig. 3(b), indicating the characteristic peaks of Cu^{1+} and Zr^{4+} from the Cu@UiO-66 system. This report elucidates the intricate balance between reaction temperature, oxidation states of Cu, and adsorption behaviours that govern the selectivity and efficiency of Cu@UiO-66 catalysts in preferential CO oxidation. Hu *et al.*[38] investigated the role of different crystal facets of CeO_2 in the dispersion of Pd single atoms and in turn in the catalytic efficiency of the Pd–CeO_2 system *N*-alkylation reaction. The group exploited NAP-XPS to elucidate the interaction between Pd single atoms and CeO_2 facets. The NAP-XPS analysis revealed that, under a reducing atmosphere, the CeO_2(100) facet generated more oxygen vacancies compared to the CeO_2(111) facet. These additional vacancies on the (100) facet effectively trapped Pd atoms, therefore promoting their atomic dispersion and preventing cluster formation. In contrast, on the (111) facet, Pd atoms were more prone to aggregation due to fewer available oxygen vacancies. This facet-dependent behaviour was directly observed through NAP-XPS (Fig. 3(c) and (d)), providing insights into the stabilization mechanisms of Pd on the CeO_2 support. On increasing the temperature, the Ce^{3+} ratio in Pd–CeO_2 increased from 25 to 41% for the (111) facet whereas for the (100) facet, the ratio increased from 28 to 46%.

Polarization-modulation infrared reflection absorption spectroscopy (PM-IRAS)

PM-IRAS is an important *in situ* technique for studying the surface chemistry, adsorption behaviour, and reaction mechanisms of SACs during heterogeneous catalysis. SACs feature higher atomic dispersion, so they exhibit more exposed active sites than other catalytic systems. PM-IRAS plays a crucial role in identifying molecular interactions and catalytic transformations at metal–support interfaces.[43] SACs offer anomalous electronic structure and coordination geometry attributed to their isolated active sites. Conventional infrared techniques struggle to effectively elucidate these sites due to low signal intensities observed during the analysis. In contrast, PM-IRAS delivers enhanced surface sensitivity, which is significant for detecting molecular adsorption over SACs. The selective polarization modulation in PM-IRAS assists in distinguishing the surface-adsorbed species from the background signals. PM-IRAS is a remarkable technique that differentiates between linear CO (M–CO) and bridge-bonded CO (M_2–CO), confirming atomic dispersion. PM-IRAS is useful in monitoring the formation of key intermediates (*e.g.*, carbonate species) during oxidation processes and in understanding the stabilization mechanisms of SACs on different support matrices. Li *et al.*[39] presented an innovative approach to designing a Pd catalyst for achieving high efficiency and selectivity in the semi-hydrogenation of acetylene to ethylene. The group proposed a unique, laterally condensed catalyst (LCC) in which a Pd layer is deposited over a specially designed SiO_2 buffer layer. PM-IRAS analysis revealed the CO adsorption over the Pd LCC catalyst to be different from that over Pd foil (Fig. 3(e)). The spectra of Pd foil revealed the variation in the CO vibration, suggesting the strong CO binding on electron-rich Pd sites. In contrast, the Pd-based LCC showcased a single bridge-bonded CO vibration, implying the presence of defect sites on which CO adsorption had taken place.

There has been substantial development in *in situ* techniques to comprehend SAC-derived CO_2RR processes; however, several bottlenecks limit a comprehensive understanding of reaction mechanisms due to various factors. For instance, most *in situ* methods, such as XAS and Raman spectroscopy, do not provide adequate spatial resolution required for the precise resolution of single-atom sites, especially when embedded within an intricate support system. Furthermore, *in situ* XAS or XPS examine the bulk region properties that do not truly reveal the actual surface sites. This hinders their capability to reveal detailed mechanisms related to interfacial charge transfer and the adsorption of reaction intermediates, which are critical processes governing the CO_2RR process. Nevertheless, *in situ* techniques have gradually become essential approaches for deciphering complex catalytic transformations and their concerted reaction mechanisms, particularly in energy conversion applications. Their ability to provide real-time, spatially resolved, and dynamic details of reaction pathways aligns well with the transition toward the optimization of materials for desired applications. Monitoring the variations in the physicochemical properties of active single atoms under operational conditions will allow researchers to optimize catalytic systems for large-scale energy conversion applications. A comparative overview categorizing different *in situ* characterization techniques used for SAC-derived CO_2RR applications can be seen in Table 1.

Single-atom catalyst-derived energy conversion applications

Anthropic actions related to technological development, economic advances, growth in population, and climatic conditions lead to a continuing increase in energy consumption. The renewable carbon cycle based on electrocatalysis is a favourable approach to concurrently alleviate the energy crisis and the greenhouse effect. However, the efficiency of energy conversion is constrained by insufficient carrier usage and deficient active sites in conventional catalysts.[44–46] SACs exhibit remarkable activity in efficiently surpassing the abovementioned obstacles. Heterogeneous SACs, in which every single metal atom is completely revealed to the surroundings and accessible for contact with reactants, are highly efficient catalysts. SACs are cost-effective as they reduce the amount of metal needed to enhance a catalytic reaction and implement advanced functions during chemical transformations. For instance, SACs enable the stability of metallic elements in mixed spin and oxidation states, providing facilitated reactivity.[47] Moreover, this characteristic is related to the exchange of noble and rare metals by earth-abundant ones, manifesting the lesser-known features that were previously enigmatic in their nanocatalyst counterparts.[48] Electrochemical CO_2RR propelled *via* renewable energy appears as a favourable technique to overcome environmental and energy-related issues by transforming CO_2 into value-added chemicals.[49] SACs consisting of isolated metal atoms with a support material exhibit tremendous activity for electrocatalytic CO_2 reduction due to their robust single-atom support contacts, remarkable catalytic performance, and maximum utilization of metal. However, SACs experience particle agglomeration, problems in large-scale generation, and low metal loading. Furthermore, the substitute for single atom-based catalysts are molecular catalysts, comprising ligand molecules linked to metal ions, having almost the same metal–nitrogen (M–N) active centres as in metal–nitrogen–carbon (M–N–C) SACs, that are greatly active for electrochemical CO_2 reduction because of their precise active sites and their alteration due to electronic and steric effects. However, molecular catalysts are confronted by moderate performance, stability and selectivity, aggregation, and poor conductivity. Several substrates have been exploited for fabricating SACs, specifically, carbon derivatives (carbon nanotubes, graphene oxide, MOF-derived nanocarbon, and g-C_3N_4),[50–53] exhibiting advantages due to their low cost, excellent electrical conductivity, specific stability and tunable surface chemistry to synthesize metal–nitrogen–carbon (M–N–C) SACs for electrocatalytic CO_2 reduction.[54] Additionally, some metal complexes (MoS_2,[55] TiO_2,[56] CeO_2,[57] TiC[58]) are also established as efficient supports for fabricating effective SACs. For instance, Zhang *et al.*[40] fabricated Ag_1 single-atom catalyst (Ag_1/MnO_2) for which HAADF-STEM (Fig. 3(f)), *in situ* XRD (Fig. 3(g)), *in situ* ETEM, and density functional theory (DFT) were utilized to characterize the evolution of Ag NPs to single atoms. The as-synthesized Ag_1/MnO_2 displayed the highest current density in the potential range of −0.6 to

Table 1 Comparative table cataloguing various *operando* characterization techniques employed in current studies of SACs for CO_2RR

In situ characterization technique	Functionality in the CO_2RR application
Aberration-corrected transmission electron microscopy (AC-TEM)	• AC-TEM enables direct visualization of single atoms, defects, and heteroatom dopants on a support material. • Highly efficient to confirm the dispersion of SACs for structure–activity correlations in CO_2RR.
Environmental transmission electron microscopy (ETEM)	• ETEM allows for real-time observation of changes in SACs and nanoparticle structures, including surface reconstruction and atom movement during CO_2RR. • Highly efficient in investigating the surface interaction of SACs with CO_2/CO and other reactants, providing valuable insight into adsorption, activation, and product formation during CO_2RR.
Scanning transmission electron microscopy (STEM)	• A highly effective technique for the study of CO_2RR that provides atomic-scale resolution for both structural imaging and elemental analysis. • By integrating methods such as energy-dispersive X-ray spectroscopy (EDS) and electron energy loss spectroscopy (EELS), STEM provides a detailed analysis of local chemical environments and elemental distributions in SACs. This facilitates the correlation between their structural characteristics, catalytic activity, and stability during CO_2RR.
Aberration-corrected high-angle annular dark-field scanning transmission electron microscopy (AC-HAADF-STEM)	This method provides atomic-resolution imaging with Z-contrast sensitivity, making it instrumental for identifying isolated single atoms dispersed on light support materials.
X-ray absorption spectroscopy (XAS)	XAS is effective for analyzing atomically dispersed single metal atoms due to its element-specific sensitivity and capability to investigate local electronic and structural environments.
Near-ambient-pressure X-ray photoelectron spectroscopy (NAP-XPS)	Unlike XPS, which requires an ultra-high vacuum, NAP-XPS enables surface-sensitive analysis under reactive gases (CO_2, H_2O) at near-operational pressures. This is useful for SACs, as the metal atoms' oxidation state and coordination can dynamically change during CO_2RR.
Polarization-modulation infrared reflection absorption spectroscopy (PM-IRAS)	PM-IRAS can be employed to track the formation of reaction intermediates on SACs during CO_2RR, showing a potential-dependent shift in the main reaction pathway and supporting the formation of products in working conditions.
In situ Raman spectroscopy	This provides molecular-level vibrational fingerprints and enables direct visualization of adsorbed intermediates such as *CO, *COOH, *HCOO, and carbonate species, which are crucial in determining product pathways and selectivity.
In situ FTIR spectroscopy	A powerful tool for investigating SAC-derived CO_2RR under real-time conditions into surface intermediates and reaction pathways under operating conditions. When integrated with electrochemical measurements, it facilitates the evaluation of intermediate adsorption on SACs at various potentials.

−1.0 V and exhibited 95.7% faradaic efficiency (FE) for CO formation, showing excellent stability for electrocatalytic CO_2 reduction with 169 mV dec^{-1} value of Tafel slope as shown in Fig. 4(a)–(d). DFT estimations revealed that single-atom Ag sites possessed high electronic density and served as the only active sites for CO_2 reduction. Hence, the Ag_1/MnO_2 electrocatalyst exhibited noteworthy activity for CO_2RR, better than that of a traditional Ag nanocatalyst ($AgNP/MnO_2$). Cai *et al.*[59] reported a novel carbon-dots-based SAC edged with special CuN_2O_2 for electrochemical CO_2 reduction. The as-prepared electrocatalyst exhibited a remarkable 78% FE and 99% selectivity for CO_2 reduction to CH_4, showing a current density of 40 mA cm^{-2}. The enhanced results were attributed to incorporating oxygen ligands, which surpassed those for most reported SACs. Moreover, theoretical simulations showed that the high activity and selectivity of CuN_2O_2 active sites were due to the surpassing of H_2 and CH_4 energy barriers and the tunable electronic framework of Cu active sites. Supported Ni catalysts are considered highly efficient for hydrogen evolution and CO_2 activation among transition metals. For instance, Millet *et al.*[60] synthesized Ni SACs with an amount of Ni up to 10 atom% and deduced it as the highest limit for the operation of SACs. STEM-HAADF images of Ni SACs before and after catalysis are depicted in Fig. 4(e)–(h). The as-synthesized Ni SACs were functioning for CO_2 activation and showed stable activity during the reaction time, which revealed linear dependency on the concentration of Ni on the surface, as shown in Fig. 4(i) and (j). It was revealed that Ni clusters were required for the CO_2RR to proceed as isolated Ni atoms were inaccessible for CO_2 conversion to CH_3OH or CH_4. The change in selectivity for CH_4 and the continuous increase of reaction rates with samples consisting of Ni clusters provided an insight into the distinct reaction durations.

Xi *et al.*[61] prepared carbon-supported Ni SACs with a coordination of 80% N dopants with metal elements. The absence of unfavourable N species was credited for the remarkable activity of optimized Ni SACs in electrocatalytic CO_2RR, which showed tremendous selectivity (~92%) and stability for the formation of CO. Guo *et al.*[62] fabricated Ni-SAC@NC for electrochemical CO_2 conversion. As-prepared SACs achieved up to ~95% FE for CO formation with a partial current density of 187.7 mA cm^{-2} at 2.7 V. The enhanced activity stemmed from defect-Ni-N_3 structure that provided more active sites in Ni-SAC@NC for CO_2 reduction.

Guo *et al.*[63] fabricated an Sn SAC (Sn-NOC) consisting of an asymmetric SnN_3O_1 configuration, which proved to be an efficient CO_2 to CO transformation electrocatalyst. The as-prepared Sn-NOC exhibited a partial current density as high as 13.9 mA cm^{-2} and 94% FE at −0.7 V for CO with improved stability as shown in Fig. 5(a)–(d). Additionally, a linear relationship was revealed between FE_{CO} and the amount of Sn–N, indicating that atomically distributed SnN_3O_1 coordination was a highly active site for CO_2RR in Sn-NOC, as displayed in Fig. 5(e). The theoretical and experimental results revealed that the asymmetric SnN_3O_1 decreased the energy barrier for the

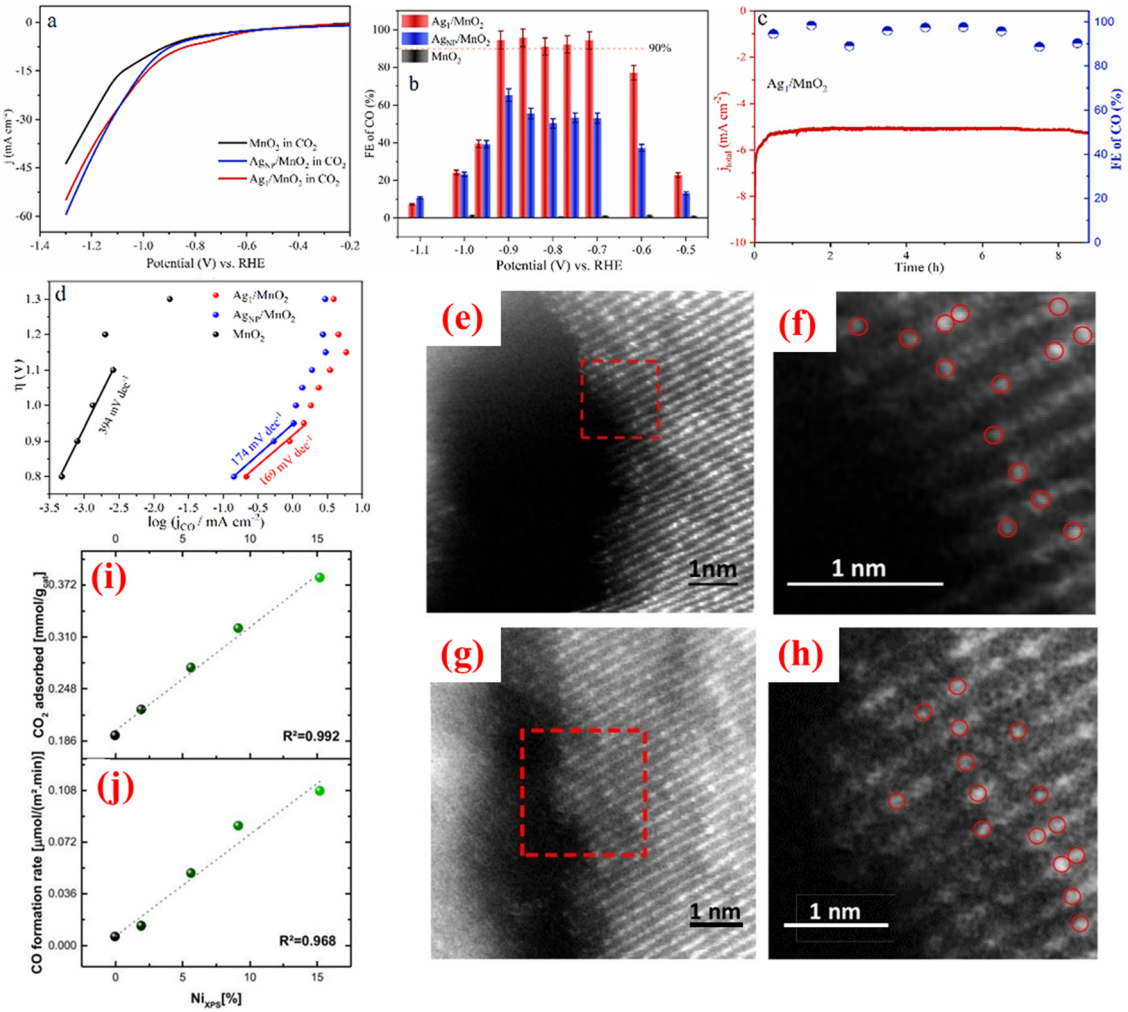

Fig. 4 (a) LSV curves, (b) FE of CO, and (c) 8-hour electrocatalytic investigations of Ag_1/MnO_2 at −0.9 V. (d) Tafel plots of as prepared catalysts. Reproduced with permission from ref. 40. Copyright 2021, John Wiley and Sons. (e) STEM-HAADF image of Ni-10% before catalysis. (f) Magnified image. (g) STEM-HAADF image of Ni-10% after catalytic investigation. (h) Magnified image. (i) Examination of CO_2 adsorbed *versus* concentration of surface nickel. (j) Investigation of CO production *versus* concentration of surface nickel. Reproduced with permission from ref. 60. Copyright 2019, American Chemical Society.

formation of CO while increasing the energy for *OCO adsorption, which is considered the main step for HCOOH formation.

Leverett *et al.*[64] studied the Cu SAC coordination for both CO_2RR and nitrate reduction reaction (NO_3RR). DFT simulations indicated that Cu–N_4 sites showed higher intrinsic performance for CO_2RR, whereas both Cu–N_{4-x}–C_x and Cu–N_4 sites were active for NO_3RR. These results assisted in merging CO_2RR and NO_3RR for the generation of urea on Cu SACs, attaining 28% FE with –27 mA cm^{-2} current density at –0.9 V. Li *et al.*[65] fabricated two kinds of In SACs, one coordinated with four nitrogen atoms (In–N_4) and the second one coordinated with three nitrogen atoms having one vacancy (In–N_3–V) to compare the electrocatalytic CO_2 activity. The In–N_3–V site exhibited the highest FE of 95% for CO production in comparison to In–N_4 (80% FE_{CO}). Theoretical calculations revealed that the structural tuning from In–N_4 to In–N_3–V brought the energies of In orbitals (s and p_z) nearer to the Fermi energy. Hence, the improved electrocatalytic performance was attributed to these hybridized orbitals that decreased the energy barrier for the formation of the COOH* intermediate. Li *et al.*[66] studied the atomic alteration of Fe SAC having phosphorus on carbon (Fe–N@P–C) for electrocatalytic CO_2 reduction. The as-prepared Fe–N@P–C showed excellent activity for CO_2 conversion to CO, achieving 98% FE and 508.8 h^{-1} turnover frequency (TOF) at 0.34 V. The results of XAS and DFT revealed that the alteration of P in Fe SAC reduced the energy barrier of *CO intermediate construction and decreased the oxidation state of the Fe centre, leading to enhanced electrochemical performance and high stability of Fe SAC. Chen *et al.*[67] investigated a sulfur-doped SAC in FeN_4 (Fe_1NSC) for electrocatalytic CO_2 reduction and characterized it *via* aberration-corrected STEM and XAS. Fe_1NSC exhibited enhanced CO_2RR activity compared with FeN_4 in the absence of sulfur, achieving 98.6% FE for CO and 1197 h^{-1} TOF. The results of theoretical analysis and *operando* characterizations verified that sulfur doping expedited H_2O activation and

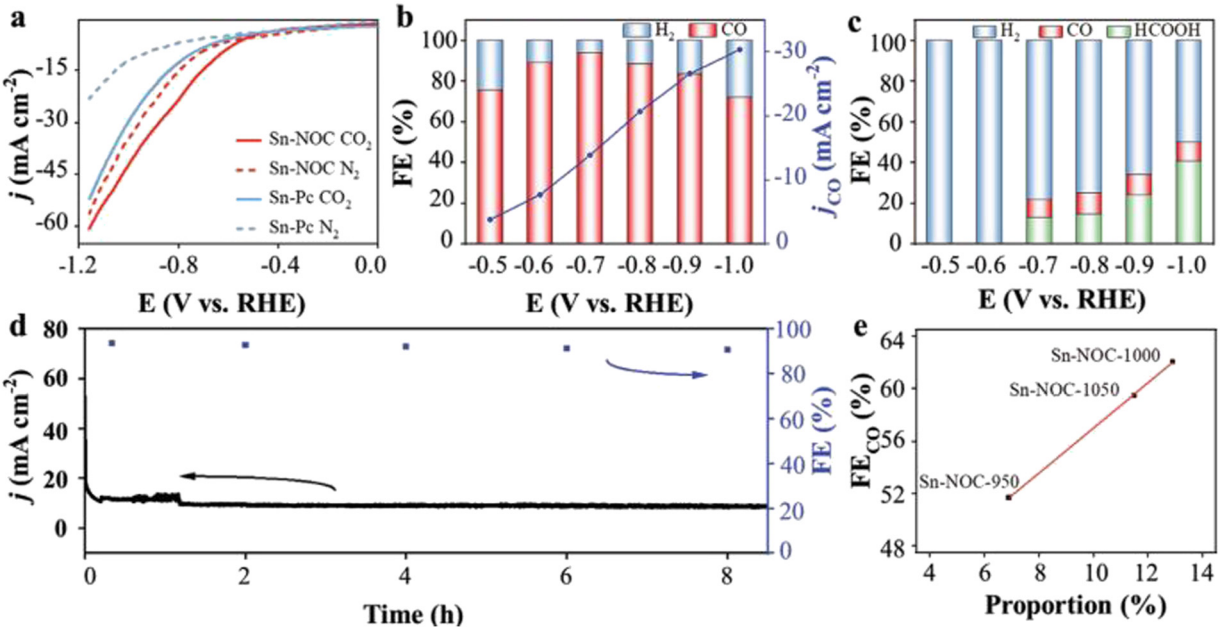

Fig. 5 (a) LSV curves of Sn-Pc and Sn-NOC in CO_2- and N_2-based electrolytes. (b) Partial current densities and FE of Sn-NOC at different potentials. (c) FE of Sn-Pc at different potentials. (d) Stability test and FE_{CO} of Sn-NOC in CO_2-based electrolyte. (e) The linear relationship between the concentration of Sn-N and FE of Sn-NOC catalysts synthesized at distinct temperatures. Reproduced with permission from ref. 63. Copyright 2021, John Wiley and Sons.

supplied enough protons for accelerating CO_2 transformation to *COOH. Lakshmanan *et al.*[68] reported Fe SAC based on three coordinated oxygens, Fe–$(O)_3$, with carbon nanotubes (Fe-n-f-CNTs) for electrochemical CO_2 reduction. The outcomes showed that Fe SACs attained 45% FE and a yield of 56.42 μmol cm^{-2} h^{-1} for C_2H_5OH formation. The catalytic characteristics decreased the reaction energy and caused the transfer of electrons to the intermediates *OCHO and *COOH, thus enhancing CO formation. The production rate of Fe SACs implied that the Fe single-atom sites generated a high amount of CO to assist the transformation of CO_2 to C_2 product. Zhang *et al.*[69] developed Ga SACs coordinated with P, S atomic surroundings showing unique features, achieving 92% FE in electrocatalytic CO_2 reduction. Theoretical calculations indicated that the versatile dynamic transition of Ga improved the adsorption energy of *COOH and upgraded the active sites over time, resulting in remarkable CO_2RR stability and selectivity. The electrochemical efficiency of different SACs toward CO_2RR application can be seen in Table 2.

Major bottlenecks and future outlook for SAC-based energy conversion

In the last few years, numerous efforts have been dedicated to single atom-based catalysts for CO_2 reduction. SACs exhibit remarkable catalytic performance due to their robust single atom–support contacts, maximum atomic utilization and uniformity of metal atoms that ensure high faradaic efficiency and lower overpotential values during CO_2RR as illustrated in Fig. 6. Fe and Ni SACs are exceptionally selective for the formation of CO with Ni-based SACs attaining higher FE, whereas Fe-based SACs show higher selectivity for CO at comparatively lower overpotentials. These are promising candidates for upcoming industrial CO_2 reduction applications. Co-based SACs are also highly active for CO_2 to CO transformation, with comparable results to those of the Fe- and Ni-based SACs. Notably, Cu-based SACs are specific materials to form products other than CO, though the generation of C_2^+ products is still in its nascent stage. Other metal-based SACs (Zn, Ag, Sn, Pb) are also potential candidates for the reduction of CO_2. Despite the progress in research concerning SACs, numerous issues need to be solved for their advancements and applications. For example, CO_2 reduction on an industrial scale is challenging due to the scarcity of efficient catalysts with notable activity and durability. Currently, the characterization of single atoms is chiefly realized by the amalgamation of XAFS, CO-DRIFT and HAADF-STEM *operando* techniques. Although these approaches provide a clear mechanistic sketch of the structure of the principal metal in a catalyst, not a single one offers the correct coordination environment and electronic structure of the single metal atoms with geometrical considerations in the working state. Hence, the current knowledge of the complex active sites of heterogeneous SACs and their mechanisms in catalytic reactions highly depends on information obtained from statistically averaged features. A promising solution for this obstacle is the utilization of single-atom electron spectroscopy, which would provide structural characterization of each metal in a microscopic range. This emerging strategy has been effectively utilized in revealing the localized electronic structure of single atoms; hence, it should be explored for gaining knowledge of the catalytic operation of isolated metal atoms.[70] Other essential work concerning SACs is to find a method that provides imaging spectroscopically or microscopically of various metal species and, at the same time, distinguishes which ones are participating in the reaction and which ones are not. Generally, variously

Table 2 The catalytic efficiency of SAC-derived electrocatalysts for CO_2RR application

Electrocatalyst	Electrolyte	Faradaic efficiency	Selectivity	Current density	Ref.
CuN_2O_2	0.5 M $KHCO_3$	78% (CH_4)	99% (CH_4)	40 mA cm^{-2}	59
Ni SACs	0.1 M $KHCO_3$	>90% (CO)	~92% (CO)	70 mA cm^{-2}	61
Ni-SAC@NC	0.5 M $KHCO_3$	~95% (CO)		187.7 mA cm^{-2}	62
Sn-NOC	0.1 M $KHCO_3$	94% (CO)	~80% (CO)	13.9 mA cm^{-2}	63
In–N_3–V	0.5 M $KHCO_3$	95% (CO)		6.7 mA cm^{-2}	65
Fe–N@P–C	0.5 M $KHCO_3$	98% (CO)			66
Fe_1NSC	0.5 M $KHCO_3$	98.6% (CO)		40 mA cm^{-2}	67
Fe-n-f-CNTs	0.5 M $KHCO_3$	45% (C_2H_5OH)			68
Ga SACs	0.5 M $KHCO_3$	92% (CO)	90% (CO)		69

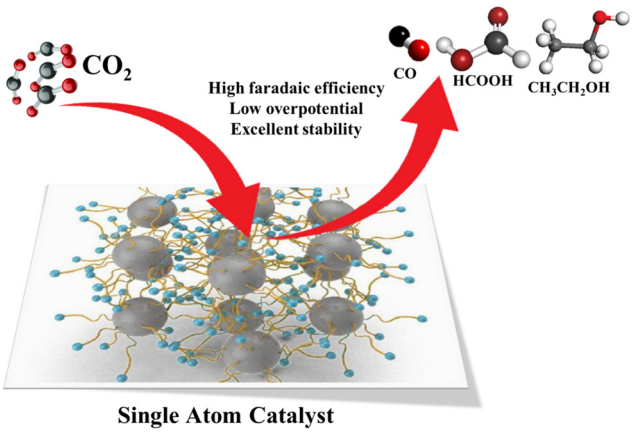

Fig. 6 Schematic illustration of SAC-derived CO_2 electroreduction into value-added chemicals.

sized metals coincide in an operating heterogeneous catalyst, and the participation of all these metals in a reaction is difficult to untangle. A single-atom material, even itself, does not show identical catalytic and structural features. It should be taken into account that most catalytic reactions are linked to the heat effect and active sites introduce a considerable change of the surrounding temperature. Lately, phonons and plasmons have been utilized to investigate the temperature of nanosystems in electron microscopy.[71] Building on these developments, a thermometry-microscopy system for catalytic applications can provide a reliable solution. As far as the CO_2RR application of SACs is concerned, a high number of single atom-based catalysts displayed unsatisfactory CO_2 reduction activity in real devices. The low solubility of CO_2 (34 mmol L^{-1}) in aqueous electrolytes and limited mass transfer of CO_2 at high current densities are limiting factors for scalable CO_2 reduction.[72] To overcome such problems single atom-based catalysts have been merged with gas diffusion layers for utilization in membrane electrode assemblies and flow cells that assist in meeting industrial needs. There are some studies reported for M–N–C SACs' exploitation at an industrial scale for CO generation in a flow cell with an excellent partial current density of more than 200 mA cm^{-2}.[73,74] Another shortcoming of SACs for CO_2RR is their moderate selectivity for C_2^+ products. Longer carbon-chain products have a higher commercial value and possess significant energy densities in comparison to their C_1 counterparts. However, the low selectivity on account of sluggish kinetics and rapid hydrogenation/oxidation of CO* before C–C coupling hampers the efficiency of C_2^+ product formation.[75] Most of the transition metal SACs (Fe, Co, Ni SACs) are highly selective for CO formation, whereas only Cu SACs generate C_2^+ products (C_2H_4, C_2H_5OH, C_3H_7OH).[76] CO_2 conversion into stable C_2^+ products is quite an issue because of the multiple electron transfer (18 and 12) required for generating C_2H_4, C_2H_5OH and C_3H_7OH.[77,78] The adjacent Cu sites can enhance CO_2 reduction into distinct hydrocarbons.[79] The two closest Cu–N_2 sites can merge with *CO to originate C–C coupling, consequently enhancing selectivity for C_2H_4, whereas other sites react to form C_1 products. Moreover, coupling Cu SACs to multiatomic sites or other metal SACs is favourable for enhancing the selectivity of C_2^+ products.

Converting CO_2 into C_2^+ *via* two steps from CO_2 to CO, followed by CO to C_2^+ can be efficient in improving the selectivity of C_2^+ due to the minimum formation of intermediates and less electron transfer. Additionally, CO_2 reduction is a difficult reaction process that involves distinct reduction routes through multi-electron transfer, thus making it challenging to understand the concerted mechanisms. To comprehend CO_2 reduction favourably with explicit active sites, aside from DFT simulations, *operando* characterization like HAADF-STEM is efficient in examining the distribution and position of single atoms on support materials, whereas Mössbauer spectroscopy, *in situ* XAS and XPS contribute in understanding the structural evolution of single atoms on a support material. Therefore, the state-of-the-art *in situ* characterizations, such as *operando* Fe Mössbauer, *in situ* Raman/FTIR/UV-Vis/XAS spectroscopy, and ETEM, are the pivotal instrumentation tools to monitor active sites and reaction pathways of CO_2RR, which in turn are beneficial to understand activity and structural relationships in SAC-based CO_2RR operations.

Conclusions

SACs have attracted significant attention for electrochemical CO_2 conversion attributed to their high atom utilization efficiency, tunable electronic structure, and excellent activity and selectivity toward CO_2RR products such as CO, formate, methanol, and ethanol. *Operando* techniques play a crucial role in understanding the structure-performance relationship of SACs during CO_2RR by allowing the real-time monitoring of metal-atom evolution, reaction intermediates, and electronic structure changes under operating conditions, providing insights

into CO_2RR mechanisms and stability of SACs. Herein, we surveyed the progress in the *in situ*/*operando* characterization techniques in elucidating the catalytic efficiency of SAC-derived catalytic systems toward electrochemical CO_2RR applications. Furthermore, we have discussed the challenges and future directions in upscaling C_2^+ products and enhancing the selectivity of SACs. We believe that combining the results of *in situ* techniques and machine learning/DFT-guided *operando* studies will pave the way for multi-faceted insights and robust catalyst design in CO_2RR applications.

Data availability

No primary research results, software or code have been included and no new data were generated or analysed as part of this review.

Conflicts of interest

The authors declare no financial competing interest.

Acknowledgements

TA thanks SERB sponsored research scheme (CRG/2023/000480) for financial support.

References

1 S. A. Ali, M. Khanam, I. Sadiq, S. Shaheen and T. Ahmad, *J. Colloid Interface Sci.*, 2025, **679**, 1046–1075.
2 K. Liu, Z. Sun, W. Chen, X. Lang, X. Gao and P. Chen, *Adv. Funct. Mater.*, 2024, **34**, 2312589.
3 S. A. Ali and T. Ahmad, *Langmuir*, 2024, **40**, 10835–10846.
4 A. Wang, J. Li and T. Zhang, *Nat. Rev. Chem.*, 2018, **2**, 65–81.
5 B. B. Sarma, F. Maurer, D. E. Doronkin and J. D. Grunwaldt, *Chem. Rev.*, 2022, **123**, 379–444.
6 Y. Duan, Y. Wang, W. Zhang, C. Ban, Y. Feng, X. Tao, A. Li, K. Wang, X. Zhang, X. Han, W. Fan, B. Zhang, H. Zou, L. Gan, G. Han and X. Zhou, *Adv. Mater.*, 2024, **36**, 2404900.
7 B. Qiao, A. Wang, X. Yang, L. F. Allard, Z. Jiang, Y. Cui, J. Liu, J. Li and T. Zhang, *Nat. Chem.*, 2011, **3**, 634–641.
8 X. Li, X. Yang, J. Zhang, Y. Huang and B. Liu, *ACS Catal.*, 2019, **9**, 2521–2531.
9 V. Muravev, G. Spezzati, Y. Q. Su, A. Parastaev, F. K. Chiang, A. Longo, C. Escudero, N. Kosinov and E. J. Hensen, *Nat. Catal.*, 2021, **4**, 469–478.
10 V. Vidal, A. Théolier, J. Thivolle-Cazat and J. M. Basset, *Science*, 1997, **276**, 99–102.
11 W. O. Haag, R. M. Lago and P. B. Weisz, *Nature*, 1984, **309**, 589–591.
12 E. Bayram, J. Lu, C. Aydin, N. D. Browning, S. Özkar, E. Finney, B. C. Gates and R. G. Finke, *ACS Catal.*, 2015, **5**, 3514–3527.
13 Z. Zhang, Y. Zhu, H. Asakura, B. Zhang, J. Zhang, M. Zhou, Y. Han, T. Tanaka, A. Wang, T. Zhang and N. Yan, *Nat. Commun.*, 2017, **8**, 16100.
14 L. Nie, D. Mei, H. Xiong, B. Peng, Z. Ren, X. I. P. Hernandez, A. DeLaRiva, M. Wang, M. H. Engelhard, L. Kovarik and A. K. Datye, *Science*, 2017, **358**, 1419–1423.
15 J. C. Liu, Y. G. Wang and J. Li, *J. Am. Chem. Soc.*, 2017, **139**, 6190–6199.
16 Y. G. Wang, D. Mei, V. A. Glezakou, J. Li and R. Rousseau, *Nat. Commun.*, 2015, **6**, 6511.
17 R. Bliem, J. E. Van Der Hoeven, J. Hulva, J. Pavelec, O. Gamba, P. E. De Jongh, M. Schmid, P. Blaha, U. Diebold and G. S. Parkinson, *Proc. Natl. Acad. Sci. U. S. A.*, 2016, **113**, 8921–8926.
18 B. Eren, D. Zherebetskyy, L. L. Patera, C. H. Wu, H. Bluhm, C. Africh, L. W. Wang, G. A. Somorjai and M. Salmeron, *Science*, 2016, **351**, 475–478.
19 Y. Liu, X. Su, J. Ding, J. Zhou, Z. Liu, X. Wei, H. B. Yang and B. Liu, *Chem. Soc. Rev.*, 2024, **53**, 11850–11887.
20 Z. Jin, P. Li, Z. Fang and G. Yu, *Acc. Chem. Res.*, 2022, **55**, 759–769.
21 K. Asakura, H. Nagahiro, N. Ichikuni and Y. Iwasawa, *Appl. Catal., A*, 1999, **188**, 313–324.
22 X. Zhang, H. Shi and B. Q. Xu, *Angew. Chem., Int. Ed.*, 2005, **117**, 7294–7297.
23 Q. Fu, H. Saltsburg and M. Flytzani-Stephanopoulos, *Science*, 2003, **301**, 935–938.
24 H. Zhao, Y. Zhu, H. Ye, Y. He, H. Li, Y. Sun, F. Yang and R. Wang, *Adv. Mater.*, 2023, **35**, 2206911.
25 E. D. Boyes, A. P. LaGrow, M. R. Ward, R. W. Mitchell and P. L. Gai, *Acc. Chem. Res.*, 2020, **53**, 390–399.
26 P. Tieu, X. Yan, M. Xu, P. Christopher and X. Pan, *Small*, 2021, **17**, 2006482.
27 X. Li, H. Y. Wang, H. Yang, W. Cai, S. Liu and B. Liu, *Small Methods*, 2018, **2**, 1700395.
28 S. Wei, A. Li, J. C. Liu, Z. Li, W. Chen, Y. Gong, Q. Zhang, W. C. Cheong, Y. Wang, L. Zheng and H. Xiao, *Nat. Nanotechnol.*, 2018, **13**, 856–861.
29 Y. Wang, C. Li, X. Han, J. Bai, X. Wang, L. Zheng, C. Hong, Z. Li, J. Bai, K. Leng and Y. Lin, *Nat. Commun.*, 2024, **15**, 5675.
30 S. H. Al-Hilfi, X. Jiang, J. Heuer, S. Akula, K. Tammeveski, G. Hu, J. Yang, H. I. Wang, M. Bonn, K. Landfester and K. Müllen, *J. Am. Chem. Soc.*, 2024, **146**, 19886–19895.
31 J. Li, Y. F. Jiang, Q. Wang, C. Q. Xu, D. Wu, M. N. Banis, K. R. Adair, K. Doyle-Davis, D. M. Meira, Y. Z. Finfrock and W. Li, *Nat. Commun.*, 2021, **12**, 6806.
32 A. Martini, D. Hursán, J. Timoshenko, M. Rüscher, F. Haase, C. Rettenmaier, E. Ortega, A. Etxebarria and B. Roldan Cuenya, *J. Am. Chem. Soc.*, 2023, **145**, 17351–17366.
33 J. Timoshenko and B. Roldan Cuenya, *Chem. Rev.*, 2020, **121**, 882–961.
34 J. Timoshenko and A. I. Frenkel, *ACS Catal.*, 2019, **9**, 10192–10211.
35 A. Zitolo, N. Ranjbar-Sahraie, T. Mineva, J. Li, Q. Jia, S. Stamatin, G. F. Harrington, S. M. Lyth, P. Krtil, S. Mukerjee and E. Fonda, *Nat. Commun.*, 2017, **8**, 957.
36 Z. Chen, A. G. Walsh and P. Zhang, *Acc. Chem. Res.*, 2024, **57**, 521–532.
37 S. Impeng, E. Salaya-Gerónimo, B. Kunkel, S. Bartling, K. Faungnawakij, B. Rungtaweevoranit and A. M. Abdel-Mageed, *J. Mater. Chem. A*, 2024, **12**, 3084–3095.
38 B. Hu, K. Sun, Z. Zhuang, Z. Chen, S. Liu, W. C. Cheong, C. Chen, M. Hu, X. Cao, J. Ma and R. Tu, *Adv. Mater.*, 2022, **34**, 2107721.
39 Z. Li, E. Öztuna, K. Skorupska, O. V. Vinogradova, A. Jamshaid, A. Steigert, C. Rohner, M. Dimitrakopoulou, M. J. Prieto, C. Kunkel and M. Stredansky, *Nat. Commun.*, 2024, **15**, 1–13.
40 N. Zhang, X. Zhang, L. Tao, P. Jiang, C. Ye, R. Lin, Z. Huang, A. Li, D. Pang, H. Yan and Y. Wang, *Angew. Chem., Int. Ed.*, 2021, **60**, 6170–6176.
41 Z. Lang, X. Wang, S. Jabeen, Y. Cheng, N. Liu, Z. Liu, T. Gan, Z. Zhuang, H. Li and D. Wang, *Adv. Mater.*, 2025, 2418942.
42 V. Muravev, G. Spezzati, Y. Q. Su, A. Parastaev, F. K. Chiang, A. Longo, C. Escudero, N. Kosinov and E. J. Hensen, *Nat. Catal.*, 2021, **4**, 469–478.
43 H. Bühlmeyer, T. Talwar, R. Eschenbacher, J. Barreto, J. Hauner, L. Knörr, H. P. Steinrück, F. Maier and J. Libuda, *ACS Appl. Mater. Interfaces*, 2024, **16**, 24063–24074.
44 S. A. Ali and T. Ahmad, *Small*, 2024, **20**, 2403401.
45 S. A. Ali, I. Sadiq, M. Estrader and T. Ahmad, *ChemCatChem*, 2025, e202500032.
46 S. A. Ali, I. Sadiq and T. Ahmad, *Nanotechnology*, 2025, **36**, 122001.
47 J. Li, H. Huang, W. Xue, K. Sun, X. Song, C. Wu, L. Nie, Y. Li, C. Liu, Y. Pan, H.-L. Jiang, D. Mei and C. Zhong, *Nat. Catal.*, 2021, **4**, 719–729.
48 Y. Zhang, J. Zhao, H. Wang, B. Xiao, W. Zhang, X. Zhao, T. Lv, M. Thangamuthu, J. Zhang, Y. Guo, J. Ma, J. Tang, R. Huang and Q. Liu, *Nat. Commun.*, 2022, **13**, 58.
49 S. A. Ali, I. Sadiq and T. Ahmad, *Langmuir*, 2024, **40**, 10414–10432.
50 A. Han, B. Wang, A. Kumar, Y. Qin, J. Jin, X. Wang, C. Yang, B. Dong, Y. Jia, J. Liu and X. Sun, *Small Methods*, 2019, **3**, 1800471.

51 Y. Cheng, S. Zhao, H. Li, S. He, J. P. Veder, B. Johannessen, J. Xiao, S. Lu, J. Pan, M. Chisholm, S. Yang, C. Liu, J. G. Chen and S. Jiang, *Appl. Catal., B*, 2019, **243**, 294–303.
52 T. Wang, Q. Zhao, Y. Fu, C. Lei, B. Yang, Z. Li, L. Lei, G. Wu and Y. Hou, *Small Methods*, 2019, **3**, 1900210.
53 J. G. Chen, *Joule*, 2018, **2**, 587–589.
54 T. Wang, Q. Zhao, Y. Fu, C. Lei, B. Yang, Z. Li, L. Lei, G. Wu and Y. Hou, *Small Methods*, 2019, **3**, 1900210.
55 R. K. Biroju, D. Das, R. Sharma, S. Pal, L. P. Mawlong, K. Bhorkar, P. Giri, A. K. Singh and T. N. Narayanan, *ACS Energy Lett.*, 2017, **2**, 1355–1361.
56 J. Wan, W. Chen, C. Jia, L. Zheng, J. Dong, X. Zheng, Y. Wang, W. Yan, C. Chen, Q. Peng, D. Wang and Y. Li, *Adv. Mater.*, 2018, **30**, 1705369.
57 Y. Wang, Z. Chen, P. Han, Y. Du, Z. Gu, X. Xu and G. Zheng, *ACS Catal.*, 2018, **8**, 7113–7119.
58 S. Back and Y. Jung, *ACS Energy Lett.*, 2017, **2**, 969–975.
59 Y. Cai, J. Fu, Y. Zhou, Y. C. Chang, Q. Min, J. J. Zhu, Y. Lin and W. Zhu, *Nat. Commun.*, 2021, **12**, 586.
60 M. M. Millet, G. Algara-Siller, S. Wrabetz, A. Mazheika, F. Girgsdies, D. Teschner, F. Seitz, A. Tarasov, S. V. Levchenko, R. Schlögl and E. Frei, *J. Am. Chem. Soc.*, 2019, **141**, 2451–2461.
61 D. Xi, J. Li, J. Low, K. Mao, R. Long, J. Li, Z. Dai, T. Shao, Y. Zhong, Y. Li and Z. Li, *Adv. Mater.*, 2022, **34**, 2104090.
62 Y. Guo, S. Yao, Y. Xue, X. Hu, H. Cui and Z. Zhou, *Appl. Catal., B*, 2022, **304**, 120997.
63 J. Guo, W. Zhang, L. H. Zhang, D. Chen, J. Zhan, X. Wang, N. R. Shiju and F. Yu, *Adv. Sci.*, 2021, **8**, 2102884.
64 J. Leverett, T. Tran-Phu, J. A. Yuwono, P. Kumar, C. Kim, Q. Zhai, C. Han, J. Qu, J. Cairney, A. N. Simonov and R. K. Hocking, *Adv. Energy Mater.*, 2022, **12**, 2201500.
65 S. Li, X. Lu, S. Zhao, M. Ceccato, X. M. Hu, A. Roldan, M. Liu and K. Daasbjerg, *ACS Catal.*, 2022, **12**, 7386–7395.
66 K. Li, S. Zhang, X. Zhang, S. Liu, H. Jiang, T. Jiang, C. Shen, Y. Yu and W. Chen, *Nano Lett.*, 2022, **22**, 1557–1565.
67 S. Chen, X. Li, C. W. Kao, T. Luo, K. Chen, J. Fu, C. Ma, H. Li, M. Li, T. S. Chan and M. Liu, *Angew. Chem., Int. Ed.*, 2022, **61**, e202206233.
68 K. Lakshmanan, W. H. Huang, S. A. Chala, B. W. Taklu, E. A. Moges, J. F. Lee, P. Y. Huang, Y. C. Lee, M. C. Tsai, W. N. Su and B. J. Hwang, *Adv. Funct. Mater.*, 2022, **32**, 2109310.
69 Z. Zhang, J. Zhu, S. Chen, W. Sun and D. Wang, *Angew. Chem.*, 2023, **135**, e202215136.
70 Y. C. Lin, P. Y. Teng, P. W. Chiu and K. Suenaga, *Phys. Rev. Lett.*, 2015, **115**, 206803.
71 M. J. Lagos and P. E. Batson, *Nano Lett.*, 2018, **18**, 4556–4563.
72 J. Zhang, W. Cai, F. X. Hu, H. Yang and B. Liu, *Chem. Sci.*, 2021, **12**, 6800–6819.
73 Z. Chen, X. Zhang, W. Liu, M. Jiao, K. Mou, X. Zhang and L. Liu, *Energy Environ. Sci.*, 2021, **14**, 2349–2356.
74 Q. Wang, K. Liu, J. Fu, C. Cai, H. Li, Y. Long, S. Chen, B. Liu, H. Li, W. Li, X. Qiu, N. Zhang, J. Hu, H. Pan and M. Liu, *Angew. Chem., Int. Ed.*, 2021, **60**, 25241–25245.
75 P. Zhu and H. Wang, *Nat. Catal.*, 2021, **4**, 943–951.
76 A. Guan, Z. Chen, Y. Quan, C. Peng, Z. Wang, T. K. Sham, C. Yang, Y. Ji, L. Qian, X. Xu and G. Zheng, *ACS Energy Lett.*, 2020, **5**, 1044–1053.
77 S. A. Ali, I. Sadiq and T. Ahmad, *Mater. Today Sustain.*, 2023, **24**, 100587.
78 I. Sadiq, S. A. Ali, S. Shaheen, I. Fatima and T. Ahmad, *Int. J. Hydrogen Energy*, 2025, **120**, 146–180.
79 A. Guan, Z. Chen, Y. Quan, C. Peng, Z. Wang, T. K. Sham, C. Yang, Y. Ji, L. Qian, X. Xu and G. Zheng, *ACS Energy Lett.*, 2020, **5**, 1044–1053.